

## MIT Open Access Articles

*Space#Based Constraints on Terrestrial Glyoxal Production*

The MIT Faculty has made this article openly available. **Please share** how this access benefits you. Your story matters.

**Citation:** Silva, Sam J. et. al., "Space#Based Constraints on Terrestrial Glyoxal Production." Journal of Geophysical Research: Atmospheres 123, 23 (December 2018): 13,583-94 doi. 10.1029/2018JD029311 ©2018 Authors

**As Published:** <https://dx.doi.org/10.1029/2018JD029311>

**Publisher:** American Geophysical Union (AGU)

**Persistent URL:** <https://hdl.handle.net/1721.1/125529>

**Version:** Final published version: final published article, as it appeared in a journal, conference proceedings, or other formally published context

**Terms of Use:** Article is made available in accordance with the publisher's policy and may be subject to US copyright law. Please refer to the publisher's site for terms of use.



## RESEARCH ARTICLE

10.1029/2018JD029311

## Key Points:

- We assess simulated global glyoxal production from six major sources
- The GEOS-Chem model captures the global spatial variability in satellite retrievals of glyoxal and formaldehyde
- Ratio of glyoxal to formaldehyde indicates that model glyoxal formation over high monoterpene-emitting regions is a factor of 3 too low

## Correspondence to:

S. J. Silva,  
samsilva@mit.edu

## Citation:

Silva, S. J., Heald, C. L., & Li, M. (2018). Space-based constraints on terrestrial Glyoxal production. *Journal of Geophysical Research: Atmospheres*, 123, 13,583–13,594. <https://doi.org/10.1029/2018JD029311>

Received 9 JUL 2018

Accepted 7 NOV 2018

Accepted article online 10 NOV 2018

Published online 5 DEC 2018

## Space-Based Constraints on Terrestrial Glyoxal Production

Sam J. Silva<sup>1</sup> , Colette L. Heald<sup>1</sup> , and Meng Li<sup>2,3</sup>
<sup>1</sup>Department of Civil and Environmental Engineering, Massachusetts Institute of Technology, Cambridge, MA, USA,

<sup>2</sup>Ministry of Education Key Laboratory for Earth System Modeling, Department of Earth System Science, Tsinghua University, Beijing, China, <sup>3</sup>Max-Planck Institute for Chemistry, Mainz, Germany

**Abstract** Glyoxal is a volatile organic compound (VOC) in the atmosphere that is a precursor to ozone and secondary organic aerosol, can be a measure of photochemical activity, and is one of a small number of VOCs observable from space. However, the global budget of glyoxal is not well understood, and there has been limited exploration of whether current chemical transport models reproduce satellite observations of this VOC. In this work we take advantage of recent advances in the retrieval of glyoxal from the Ozone Monitoring Instrument along with retrieved formaldehyde and the GEOS-Chem model to constrain global glyoxal sources. Model glyoxal is produced by direct emissions from fires (6.5 Tg/year) and secondary chemical production (32.9 Tg/year) from biogenic and anthropogenic precursors. The model reproduces the annual average terrestrial spatial variability in formaldehyde and glyoxal reasonably well, with an  $R^2$  of 0.8 and 0.5, respectively. We find that the model representation of biomass burning,  $C_2H_2$ , glycolaldehyde, and isoprene-dominated glyoxal production is consistent with the observations of glyoxal and formaldehyde, and the ratio of glyoxal to formaldehyde to within ~20%. However, the observations suggest that glyoxal production from the high monoterpene-emitting boreal regions is underestimated in the model, with concentrations low by more than a factor of 3. This suggests that the oxidative chemistry of monoterpenes is not well represented in the GEOS-Chem model and that more laboratory work is needed to constrain the impact of monoterpene emissions on atmospheric composition.

## 1. Introduction

Glyoxal ( $C_2H_2O_2$ ) is the smallest and one of the most abundant dicarbonyls in the atmosphere. It is emitted from biomass burning and formed from the oxidation of precursor volatile organic compounds (VOCs; Fu et al., 2008). In the atmosphere, glyoxal undergoes chemical oxidation and photolysis, which ultimately leads to the production of both ozone and particulate matter (PM; Knute et al., 2014). Ozone and PM are the leading contributors to poor air quality, exposure to which is estimated to cause the premature deaths of over 4 million people per year (Cohen et al., 2017). Ozone and PM also both alter the radiative balance of the Earth, with potential impacts on regional weather and climate (Intergovernmental Panel on Climate Change, 2013). Furthermore, given that glyoxal is largely chemically produced in the atmosphere, it is also a potential indicator of oxidative chemistry, providing constraints on the transformations of other key atmospheric VOCs (e.g., isoprene). Over the past 15 years, advances in retrieval methodology and instrument design have enabled detection of glyoxal by space-borne UV-visible spectrometers. The global view that satellites provide presents a valuable opportunity to constrain worldwide glyoxal sources.

Given its short atmospheric lifetime (~3 hr) and the relatively small source of direct emissions, glyoxal is frequently used as a measure of local photochemical activity and VOC chemistry (Volkamer et al., 2005). This is particularly useful in regions with large emissions and formation of VOCs such as cities, where VOC chemistry can otherwise be obscured by large direct emissions (Volkamer et al., 2007). For example in Beijing, Yang et al. (2018) found that glyoxal can be a measure of ROx radical formation, atmospheric oxidation, and ozone formation. On the global scale, Vrekoussis et al. (2009) demonstrated that satellite observations of glyoxal are consistent with large biogenic, biomass, and anthropogenic source regions.

In addition to using glyoxal measurements alone to assess VOC chemistry, several studies have demonstrated the complementary information that formaldehyde ( $CH_2O$ ) can provide. Wittrock et al. (2006) made the first global assessment of glyoxal and formaldehyde using satellite data from SCIAMACHY, demonstrating the potential for these observations to constrain many VOC sources, including isoprene, biomass burning, anthropogenic, and oceanic emissions. These constraints were further refined by Vrekoussis et al. (2009, 2010), who

used SCIAMACHY and GOME-2 retrievals of glyoxal and formaldehyde, along with the ratio of glyoxal to formaldehyde (RGF) to classify regions by their dominant VOC sources: anthropogenic, biogenic, or pyrogenic. Surface observations of the relative abundance of these species have also been used as a source indicator; for example, DiGangi et al. (2012) found that differences in surface RGF in remote regions corresponded to different source types. However, retrieved RGF from the SCIAMACHY and GOME-2 instruments disagreed with aircraft and surface observations, with different RGF thresholds associated with various sources when assessed from a satellite (DiGangi et al., 2012; Kaiser et al., 2015). Satellite and aircraft observations indicated decreasing RGF with anthropogenic influence, whereas surface-based RGF increased with anthropogenic influence (DiGangi et al., 2012; Kaiser et al., 2015). This disparity challenges the value and overall interpretability of the RGF when used to constrain VOC sources, and the reasons behind the disagreement between space- and surface-based RGF remains unclear (Kaiser et al., 2015), though differences in the observed vertical extent in RGF (e.g., free troposphere versus boundary layer) and satellite interferences are likely contributors (DiGangi et al., 2012; Chan Miller et al., 2014). Recently, a glyoxal retrieval from the Ozone Monitoring Instrument (OMI) was developed by Chan Miller et al. (2014), which when combined with OMI formaldehyde retrievals, was more consistent with surface-observed RGF (Chan Miller et al., 2014; Kaiser et al., 2015). The OMI retrieval potentially reproduces surface-based RGF observations better due to a lower sensitivity to water vapor and a carefully selected reference sector correction.

Despite these recent advances, there is still limited information on the chemical production of glyoxal at the global scale. Myriokefalitakis et al. (2008) used the TM4 model to simulate glyoxal abundance and formation, but they did not characterize the direct chemical precursors responsible for the glyoxal production; rather, they investigated several large emission source categories (e.g., anthropogenic and biogenic). Fu et al. (2008) developed the first glyoxal simulation using the GEOS-Chem model, including an assessment of the chemical budget, and showed qualitative agreement with the spatial patterns reported by the SCIAMACHY satellite observations. However, the fidelity of global glyoxal production in chemical transport models has yet to be formally tested. While the previous studies show broad agreement with observed concentrations, that alone does not confirm a correct representation of glyoxal production. Given that glyoxal concentrations are a convolution of chemical formation and precursor emissions strength, compensating biases in each may lead to an unbiased simulations of concentration.

In this work we investigate a model representation of glyoxal production at the global scale. We go beyond previous work by explicitly tracing the production of glyoxal from five major direct chemical precursors along with direct emissions from fires and compare the simulated abundance and RGF over dominant source regions to satellite observations. We treat the OMI observations of formaldehyde and glyoxal as qualitatively appropriate measures for model assessment but are cautious with quantitative evaluations given that the characterization of their respective accuracy and precision has not been completed at the global scale (Duncan et al., 2014).

## 2. Model Description

We use the global chemical transport model GEOS-Chem v11-02c ([www.geoschem.org](http://www.geoschem.org)) to investigate the chemical sources of terrestrial VOCs. We use the global configuration of the model at  $2^\circ \times 2.5^\circ$  horizontal resolution, with 47 vertical levels, from the surface through the stratosphere. The model is driven by MERRA-2 meteorology from the Global Modeling and Assimilation Office (Gelaro et al., 2017) for the year 2005.

GEOS-Chem contains a detailed  $\text{HO}_x\text{-NO}_x\text{-VOC-O}_3$  chemical mechanism (Bey et al., 2001; Mao et al., 2013; Travis et al., 2016). Glyoxal in GEOS-Chem is chemically formed as described by Fu et al. (2008), through the oxidation of aromatics (benzene, toluene, and xylenes), glycolaldehyde, isoprene, monoterpenes, and acetylene. Glyoxal formation from aromatics follow Fischer et al. (2014) with first-generation yields of  $\sim 25\%$  when oxidized by OH. Isoprene and glycolaldehyde formation of glyoxal in the model is described in detail in Chan Miller et al. (2017), with  $\text{NO}_x$ -dependent yields ranging from 1% to 7%, depending on OH exposure time. Monoterpene chemistry follows Fisher et al. (2016) and Atkinson and Arey (2003), with two lumped species representing species with one double bond ( $\alpha$ -pinene) and two double bonds

**Table 1**  
*The Global Emissions of Key Species Used in the GEOS-Chem Simulation for the Year 2005*

Key species	Emissions (Tg/year)
Glyoxal	6.5
Isoprene	368.7
Acetylene	2.7
Ethylene	27.9
Monoterpenes	118.9
Aromatics	29.9
Glycolaldehyde	1.3
CO	921.0
NO <sub>x</sub>	116.8

(limonene). We assume a constant molar yield of 5% glyoxal from both lumped monoterpenes when oxidized by O<sub>3</sub>, in line with Fu et al. (2008). Acetylene and ethylene glyoxal formation was added following Safieddine et al. (2017), with a 65% glyoxal yield from the oxidation of acetylene by OH. Glyoxal forms from ethylene through a multigenerational oxidation process initiated by oxidation with OH (Safieddine et al., 2017). The reaction rates of acetylene and ethylene are updated here to match those from the Jet Propulsion Laboratory data evaluation (Burkholder et al., 2015). Formaldehyde is chemically formed through the oxidation of methane as well as a myriad of VOC precursors from biogenic, biomass burning, and anthropogenic sources (Fu et al., 2007; Marais et al., 2014). Isoprene chemistry, including the formation of formaldehyde and glyoxal, has been substantially updated and constrained in a series of studies using

observations from the Studies of Emissions and Atmospheric Composition, Clouds and Climate Coupling by Regional Surveys (SEAC<sup>4</sup>RS) aircraft campaign in the southeast United States (Chan Miller et al., 2017; Fisher et al., 2016; Travis et al., 2016). Key updates include chemistry changes relating to isoprene nitrates (Fisher et al., 2016), organic aerosol formation (Marais et al., 2016), and glyoxal formation (Chan Miller et al., 2017). These updates improve the agreement between simulated mixing ratios of both glyoxal and formaldehyde with observations in the southeast United States (Chan Miller et al., 2017; Marvin et al., 2017). Losses of glyoxal include photolysis, oxidation, dry and wet deposition, and irreversible heterogeneous aerosol uptake, from Marais et al. (2016) with a daytime uptake coefficient of  $2.9 \times 10^{-3}$  and a nocturnal uptake coefficient of  $5 \times 10^{-6}$ .

Global anthropogenic emissions in GEOS-Chem include the EDGARv4.2 inventory (<http://edgar.jrc.ec.europa.eu>), with aromatics and C<sub>2</sub>H<sub>x</sub> compounds from the RETRO emissions inventory (Schultz et al., 2007). Aircraft emissions are from the AEIC inventory (Stettler et al., 2011; Simone et al., 2012). Regional anthropogenic emissions are used where available, including NEI2011v1 over the United States (Environmental Protection Agency National Emissions Inventory, 2015), and MEIC v1.2 over China ([www.meicmodel.org](http://www.meicmodel.org); Li et al., 2014; Li et al., 2017). Updated emissions generated by the MEIC model were included in GEOS-Chem for the glyoxal precursors (benzene, toluene, xylenes, acetylene, and ethylene) following Li et al. (2014), with emissions for the year 2006. Biogenic emissions are calculated online from the MEGANv2.1 emissions framework, consistent with Guenther et al. (2012). Biomass burning emissions, including formaldehyde and glyoxal, are from the GFED4 emissions inventory (Giglio et al., 2013), with updated glyoxal emission factors for agricultural burning of 0.0016 relative to CO following Zarzana et al. (2017). Hourly and daily scale factors were applied to the fire emissions following Mu et al. (2011). Emissions for 2005 of glyoxal precursors and other key species are summarized in Table 1. The overall uncertainties in these emissions are not well characterized and vary based on source type (e.g., 30% for anthropogenic NO<sub>x</sub> over China [Li et al., 2017], as compared to a factor of 2 for biogenic isoprene emissions [Guenther et al., 2012]).

### 3. Satellite Data

We compare our model simulation with satellite retrievals of glyoxal and formaldehyde from the OMI (Chan Miller et al., 2014; González Abad et al., 2015). OMI is on board the National Aeronautics and Space Administration (NASA) Aura platform (launched in 2004) and achieves global coverage in ~3 days with an overpass of ~1300 local time and a swath size of  $13 \times 24$  km<sup>2</sup> at nadir. For both glyoxal and formaldehyde retrievals, we apply the recommended best quality control screening contained within the data file quality flags and remove all retrievals with cloud fraction larger than 20% and solar zenith angle larger than 70°. We also remove scenes from the edges of the swath due to their very large width (similar to Surl et al., 2018). Both retrievals are converted from slant columns to vertical columns using the air mass factor formulation, which accounts for instrument geometry, the vertical profile of the target gas species, and atmospheric scattering (Palmer et al., 2001). We recalculate and apply updated air mass factors using the GEOS-Chem model vertical profiles simulated here (matched to the date and location of the retrieval) and scattering weights provided with the satellite retrievals to enable a direct comparison between our simulations and the observations (Duncan et al., 2014). This air mass factor correction leads to substantial

changes in the retrieved glyoxal concentrations (upward of 20%) between the original and updated vertical column, due to large differences between the temporally matched profiles from our updated model and the monthly average climatologies provided with the OMI product. The updated air mass factor has a relatively smaller impact on formaldehyde (~5%). In the year 2007, an issue with the OMI known as the “row anomaly” removed a large fraction of the usable pixels, substantially reducing the number of high-quality retrievals. In this work, we use data from the year 2005, prior to this row anomaly, to take advantage of the large number of available observations.

The glyoxal satellite retrievals are from the Smithsonian Astrophysical Observatory, as described in Chan Miller et al. (2014). These retrievals have been used in previous work to understand the distribution of glyoxal from isoprene emissions in the southeast United States (Chan Miller et al., 2017) and aromatic emissions in the Pearl River Delta (Chan Miller et al., 2016), as well as to motivate future work constraining VOC speciation from space using the RGF (Kaiser et al., 2015). Due to the relatively small spectral signature of glyoxal, the retrievals have low precision, with large relative uncertainties ( $\pm 104$ – $401\%$ ) on a per-retrieval basis, and have a 1 sigma detection limit of  $0.2$ – $1 \times 10^{14}$  molecules/cm<sup>2</sup>. We mitigate the large uncertainty by spatially and temporally averaging all observations to the GEOS-Chem  $2^\circ \times 2.5^\circ$  grid on a monthly basis. Due to issues with spectral autocorrelation with spectra of liquid water, glyoxal retrievals over oceans are systematically negative; thus, we focus our analysis over land to avoid these issues. The accuracy of these retrievals have not yet been fully validated, though initial comparisons demonstrate that they agree better with in situ observations as compared to previous glyoxal retrievals (Chan Miller et al., 2017; Kaiser et al., 2015). However, potential issues with surface reflectance could be responsible for biases as large as a factor of 2 (Chan Miller et al., 2017).

The formaldehyde retrievals are from the NASA OMHCHOv003 data product (González Abad et al., 2015). The relative uncertainties per vertical column of formaldehyde are lower than glyoxal, but still substantial ( $\pm 50$ – $105\%$ ), with a detection limit of  $1 \times 10^{16}$  molecules/cm<sup>2</sup>. We apply the same spatial and temporal averaging to this data set. These retrievals have been used extensively to constrain VOC precursors, including biogenic isoprene emissions over the southeast United States (Kaiser et al., 2018) and VOCs over India (Surl et al., 2018). Recent work over the southeast United States found that this retrieval is biased low in that region (Zhu et al., 2016), potentially related in part to issues with the assumed scattering weights and surface reflectance. According to Zhu et al. (2016), there is no evidence to suggest that this bias is regionally specific, so we multiply all formaldehyde retrievals by a constant factor of 1.59 to account for this bias as recommended by Zhu et al. (2016). We comment on whether our comparisons support this scaling factor in section 5.

Given the large variability and random noise in the satellite products, and without a global direct validation of the OMI glyoxal retrieval, a robust assessment of the model biases in absolute magnitude is not possible given potential unquantified bias and skew in the observations. We focus here on assessing the relative variability of the model simulations as compared to the observations and do not emphasize disagreements in overall magnitude, treating the satellite observations as qualitatively correct.

#### 4. Global Simulation of Glyoxal and Formaldehyde

We simulate the global abundance of both glyoxal and formaldehyde to investigate their potential constraints on terrestrial glyoxal chemical formation. The simulated seasonal concentrations of both species are shown in Figure 1. Both species show large and consistent signatures of anthropogenic sources in China and biogenic sources throughout the tropical forests, as well as tropical fires. The seasonal peaks in the tropics largely reflect the fire seasons. The spatial variability in the midlatitudes is driven by both vegetation dynamics and seasonal changes in actinic flux. Since formaldehyde and glyoxal are both photochemically produced, the seasonality in Figure 1 is a convolution of direct emissions, photochemical activity, and precursor VOC abundance. To disentangle these effects in a computationally efficient way, previous studies have implemented sensitivity studies by adding and removing entire classes of emissions or formation pathways (e.g., “turning off” biogenic emissions, Myriokefalitakis et al., 2008). While this technique can provide qualitative insight into sources, it perturbs model oxidation substantially. Given the small number of chemical sources of glyoxal, we are able to directly quantify all chemical formation pathways of glyoxal, without perturbing the model chemistry. This is not practical to do for formaldehyde, due to the



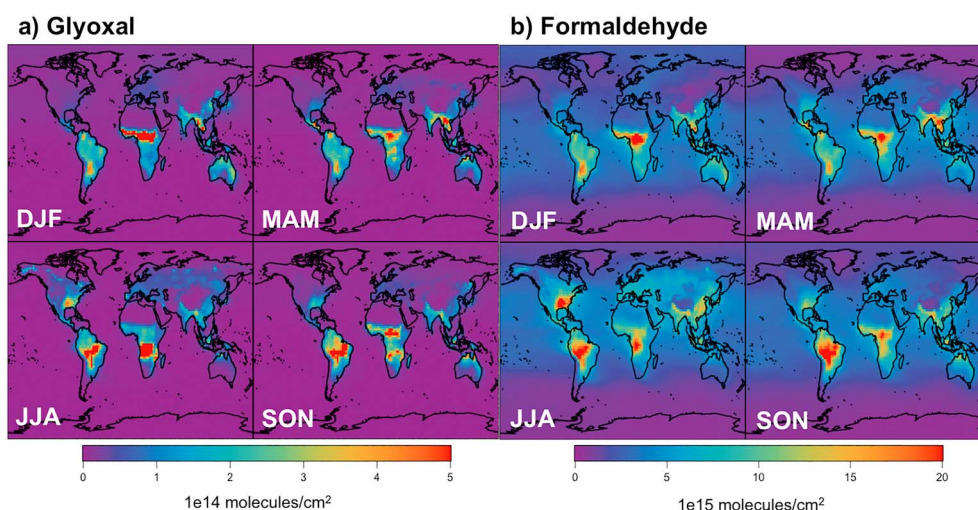


**Figure 1.** The seasonal average column concentrations of (a) glyoxal and (b) formaldehyde as simulated by the GEOS-Chem model for 2005. DJF = December/January/February; MAM = March/April/May; JJA = June/July/August; SON = September/October/November.

considerable number of formation pathways present in the GEOS-Chem chemical mechanism. Previous studies have characterized the global formaldehyde budget and found that the global burden is strongly controlled by methane oxidation (~78%), with the remainder directly emitted from mostly fires and anthropogenic activity (2%) or formed from chemical precursors (20%) (Fortems-Cheiney et al., 2012); the latter is generally thought to be dominated by isoprene. In GEOS-Chem, all of the glyoxal precursors also produce formaldehyde, with the exception of  $C_2H_2$ .

Table 2 summarizes the glyoxal budget as simulated for the year 2005 with the GEOS-Chem model. While the GEOS-Chem mechanism has been substantially updated in the v11-02 release, particularly for isoprene, the overall budget of glyoxal remains consistent with previous work (Fu et al., 2008), with ~85% of all glyoxal produced in the atmosphere, ~90% lost to chemical processes, and a lifetime of 3 hr. Given recent work demonstrating that model emission factors of glyoxal are too high over agricultural fires (Zarzana et al., 2017), which we have adjusted here, and a lack of updated information on other fuel types, the 6.5 Tg/year (15%) of glyoxal pyrogenically emitted in this study is potentially a high estimate. In total, biogenic sources contribute more than 50% of all glyoxal chemical production, with the remainder composed of anthropogenic and biomass burning precursor emissions.

Annual mean maps of the relative strength of each of the precursors from Table 2 are shown in Figure 2, where the local production from a given precursor was divided by total production. The dominant precursor over vegetated land is isoprene, with modest influence of monoterpenes over boreal forests during the summer months. Aromatics are most important in two largely anthropogenic regions, Europe and China. Direct emissions of glyoxal from fires have the strongest influence on glyoxal sources over the Congo and spatially heterogeneously over high-latitude boreal forests. Acetylene is most dominant over the remote oceans and near coastal regions, which are excluded from further analysis due to large uncertainties in the quality of the glyoxal retrievals over those areas.

**Table 2**

*The Global Glyoxal Budget as Simulated by GEOS-Chem for the Year 2005*

Production (Tg/year)	39.4
Glyoxal	6.5
Isoprene	16.5
Acetylene	3.4
Monoterpenes	0.8
Aromatics	4.8
Glycolaldehyde	7.5
Sinks (Tg/year)	39.4
Wet deposition	1.8
Dry deposition	1.9
Oxidation and photolysis	35.7
Glyoxal burden (Gg)	14.3
Glyoxal lifetime (hr)	3.2

## 5. Satellite-Based Assessment of Model Simulation

We use the OMI satellite observations of glyoxal and formaldehyde discussed in section 3 to assess our model simulation. Annual average spatial comparisons (over land only) are shown in Figure 3, alongside

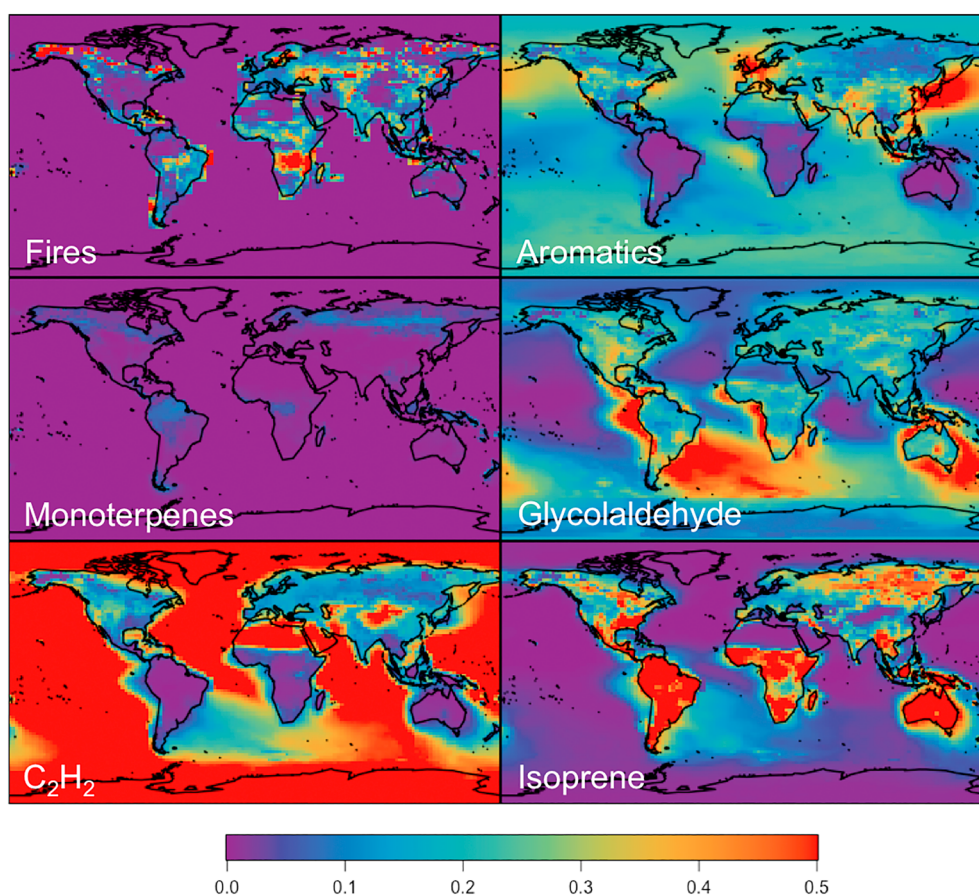


**Figure 2.** The annual average relative contribution of glyoxal sources as simulated by GEOS-Chem for the year 2005, calculated as the ratio of the source divided by the total source in the atmospheric column.

global maps of both observed formaldehyde and glyoxal. The model reproduces the observed annual average terrestrial formaldehyde reasonably well, with a reduced-major-axis (Hirsch & Gilroy, 1984) slope of  $\sim 0.8$  and an  $R^2$  of 0.8. On the whole, scaling the observed formaldehyde by a factor of 1.59 following Zhu et al. (2016), as done here, leads to a modest global underestimation of the model, which would otherwise substantially overestimate the observations (slope of  $\sim 1.4$ ). These results are consistent with the performance of many other chemical mechanisms, as tested by Marvin et al. (2017) in the southeast United States. The major terrestrial hotspots in formaldehyde visible in Figure 3 are the isoprene and biomass burned sources in the tropics, anthropogenic emissions in East Asia and Europe, and the isoprene signatures from forests in the midlatitudes.

The annual average simulated terrestrial glyoxal does not match OMI observations quite as well, with a reduced-major-axis slope of 0.9 and an  $R^2$  of 0.5. Both the model and the observations reflect similar hotspots throughout regions with large anthropogenic, biogenic, and pyrogenic sources. Though the model is relatively consistent with observations globally, there is a latitudinal shift in the location of the major African fire hotspot, and simulated concentrations over both China and Europe are generally lower than observed. According to our model simulation, glyoxal over China and Europe are dominated by formation from aromatics, glycolaldehyde, and direct emissions, suggesting that one or several of these sources is underestimated in this regions. The relative lack of skill in simulating glyoxal as compared to formaldehyde is obvious from Figure 3 and suggests that the model description of processes governing glyoxal formation and abundance may be inaccurate or incomplete.

Despite the underestimation over China, the addition of the MEIC emissions inventory described in section 2 improved the model relative to the base version. The monthly spatial correlations between the model and

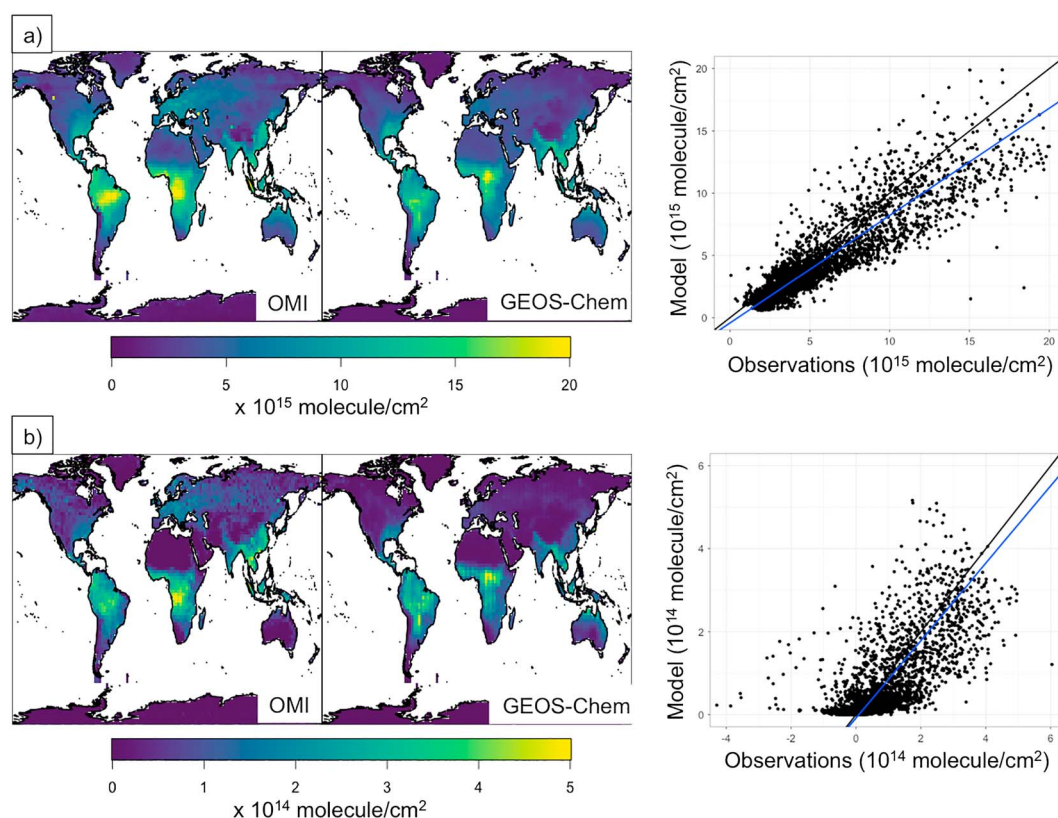


**Figure 3.** Annual OMI-retrieved and GEOS-Chem-simulated (a) formaldehyde and (b) glyoxal column concentrations for 2005, alongside scatterplot spatial comparisons. The black lines are 1:1, and the blue lines are a reduced-major-axis line of best fit. OMI = Ozone Monitoring Instrument.

the OMI glyoxal observations over China increase by 5–10% (median of 0.44 to 0.50) during most months when the MEIC emissions are used as compared to using the base emissions from Yevich and Logan (2003) and RETRO (Schultz et al., 2007).

We evaluate the simulated chemical VOC production by comparing the modeled and observed concentrations of formaldehyde and glyoxal, as well as RGF over large source regions. Large source regions were defined using simulated monthly production values, wherein we selected locations with the largest relative production from a given pathway for the year 2005. The largest relative production was calculated as locations in the upper 25th percentile of the absolute production from a given pathway (e.g., molecules glyoxal from isoprene) and in the upper 25th percentile of relative production (e.g., the ratio of molecules glyoxal from isoprene divided by total local production, as plotted in Figure 2). We exclude monthly mean observations of less than  $0.1 \times 10^{13}$  molecules/cm<sup>2</sup> to avoid including observations well below the detection limit that may be dominated by measurement uncertainties. We constrain the monoterpene regions to be above 40° latitude to focus on boreal forests, where other non-monoterpene sources are relatively much smaller and require all C<sub>2</sub>H<sub>2</sub> production to be north of Antarctica. Maps of the production locations are shown in Figure 4, colored by the number of months used in a given location. Since we filter for regions in the upper quartile in both absolute and relative emissions, these selection maps do not directly match the production maps in Figure 2; that is, absolute glyoxal production in a given location may not be dominated by this pathway. Instead, we select for areas with the highest production from a given pathway and the lowest influence of other sources to reduce the influence of confounding sources. For example, the biomass burning emissions regional selection favors Eastern Europe over the tropics due to a relatively smaller influence of other production pathways, particularly isoprene. The variability in the monthly selection represents the seasonal cycle in many of the precursor emissions. For the isoprene-dominated regions, the boreal forests and southeast United States are only selected in the summer months, when biogenic activity is largest,



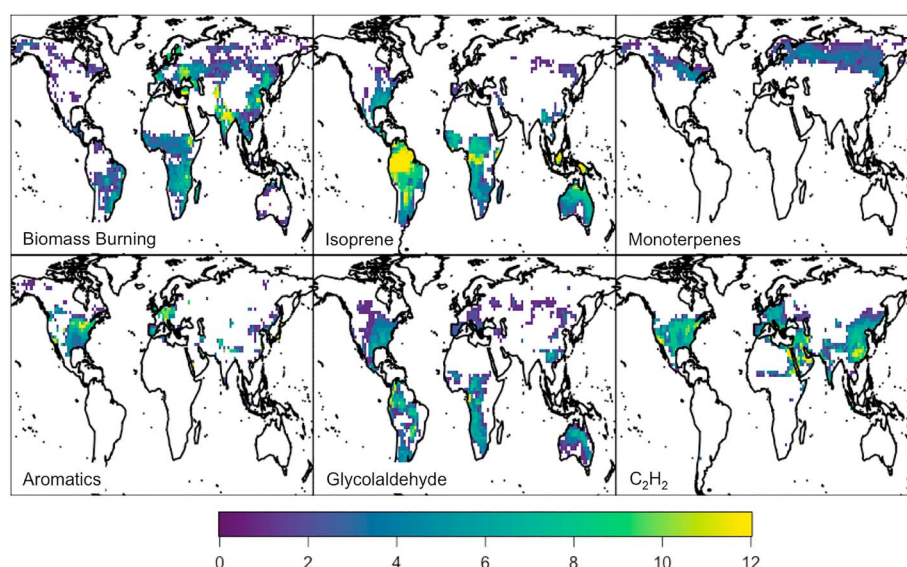


**Figure 4.** The glyoxal source regions where contributions from a specific precursor are largest, globally, for the year 2005, as simulated by GEOS-Chem. The color represents the number of months used in a given location.

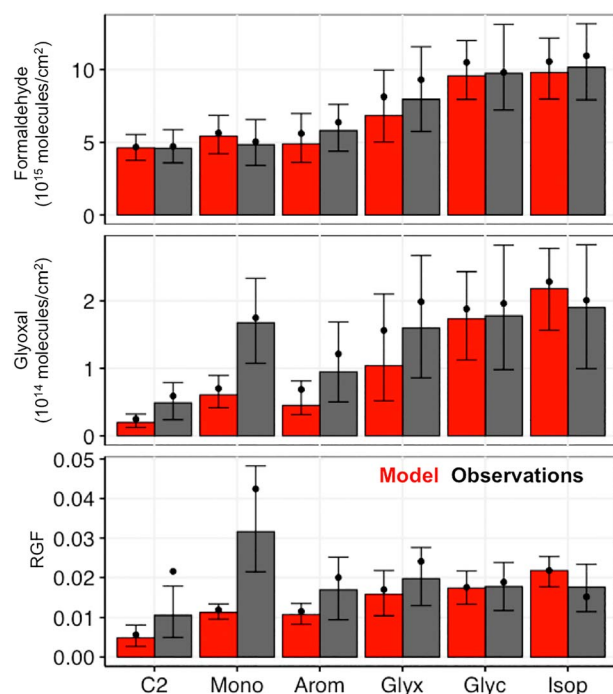


**Figure 5.** Average column concentrations of formaldehyde, glyoxal, and the RGF for all six dominant glyoxal source regions (see Figure 4 for the regions) as simulated by GEOS-Chem (red) and observed by OMI (black) in 2005. The bars are at the median value, error bars correspond to the interquartile range (25th–75th percentiles), and points represent the mean. Sources are abbreviated as follows: C2 =  $C_2H_2$ ; Mono = monoterpenes; Arom = aromatics; Glyx = direct emissions of glyoxal from fires; Glyc = glycolaldehyde; and Isop = isoprene. RGF = ratio of glyoxal to formaldehyde.

whereas the tropics are selected year-round. The  $C_2H_2$ -dominated regions are the most spatially homogeneous, with many locations selected for 1 month, when all other regional sources are small. In total, this filtering results in at least 1.2 million model/observation pairs for each production pathway in the year 2005. We note that there may be inaccuracies in this classification methodology due to inaccuracies in the GEOS-Chem model representation of glyoxal. However, it is the best estimation of all six dominant sources, given the lack of any other consistent information.

Figure 5 summarizes the mean concentration and RGF over the six regions shown in Figure 4, along with the interquartile ranges. We show interquartile ranges over confidence intervals because the large number of observations in each region leads to small confidence intervals, which understate the overall spread in the observations. From Figure 5 it is apparent that the overall observed abundance of both formaldehyde and glyoxal varies substantially across dominant source regions. For both VOCs, the smallest concentrations are observed over the  $C_2H_2$ -dominated regions, and the largest concentrations are over isoprene- and glycolaldehyde-dominated locations, with chemical formation from aromatic precursors and monoterpenes as well as direct emissions from fires as intermediates across the distribution. The regions dominated by production from  $C_2H_2$  are all remote, or during low absolute VOC production months, which leads to the small overall magnitude.

The model generally reproduces the observed mean concentrations of formaldehyde over all six large source regions to within 10%, consistent with a relatively robust formaldehyde simulation. The same is not true of glyoxal, where there is substantial departure between the simulated and satellite-retrieved concentrations over regions with the highest production of glyoxal from monoterpenes. In other regions, the relative magnitude is consistent between the observed and modeled results. The lowest values are over  $C_2H_2$  and aromatic precursor locations, and higher values coincide with fires, isoprene, and glycolaldehyde formation. The

model underestimation of glyoxal over Europe (and likely China) is explained in part by the low glyoxal concentrations associated with aromatic precursors.

While the comparison of average concentrations is a useful diagnostic of model performance, it is limited in terms of assessment of VOC production due to the convolution with the precursor emissions strength. We investigate whether the RGF is informative as a space-based constraint on VOC chemistry (eliminating some of the impact of potentially biased emissions) and then assess model performance in simulating RGF.

Figure 5 shows that satellite-observed RGF does not differentiate well between aromatic, fire, glycolaldehyde, and isoprene sources (RGF 0.016–0.019). The only precursors that produce distinctive RGF values are monoterpene-dominated boreal forests (0.031) and  $C_2H_2$  chemistry (0.011). The very high observed RGF over monoterpene-dominated regions and the moderate (0.018) RGF over isoprene-dominated regions are both consistent with previous literature (Chan Miller et al., 2014; Kaiser et al., 2015). It is important to note that since we are characterizing formation associated with the precursor and not emitted species, these results are not directly comparable with previous research that focuses on anthropogenic versus natural sources (DiGangi et al., 2012; Vrekoussis et al., 2009, etc.) because the precursors  $C_2H_2$ , glycolaldehyde, and aromatics all come from a variety of natural and anthropogenic sources. However, we do not observe any of the very high RGF values ( $>0.4$ ) reported over large anthropogenic sources (Kaiser et al., 2015) associated with any large production pathway.

While the observed RGF is similar across regions dominated by aromatics, fires, glycolaldehyde, and isoprene, the simulated RGF for these same regions shows a greater spread, with RGF values over isoprene-dominated regions (0.021) markedly higher than RGF values over aromatic-dominated regions (0.011). Given the large variability and potential unknown biases in the retrieved glyoxal concentrations, it is not evident if this difference is indicative of pervasive model chemical formation issues. Overall, this disparity is small relative to the very large disagreement over monoterpene-dominated regions, where the model RGF strongly underestimates observed RGF in both relative rank and overall magnitude (a factor of 3). The three contributing sources in the monoterpene-dominated regions are monoterpene oxidation, biomass burning, and isoprene oxidation (see Figure 2). The broad agreement in formaldehyde concentrations implies that the disagreement is not related to the overall magnitude of the biogenic and biomass burning precursor emissions. Additionally, recent work by Zarzana et al. (2017) suggests that model glyoxal emissions from agricultural fires are too high. If that overestimate were present for other fuel types, it would drive the model RGF even lower. We can therefore surmise that the overestimation is not associated with direct emissions of glyoxal and its precursors and instead likely related to glyoxal chemical formation. Given that regions where the formation from isoprene dominates glyoxal concentrations are all relatively well represented by the model, we conclude that there is likely a substantial model underestimation of glyoxal formation from monoterpene chemistry. As stated in section 2, the monoterpene oxidation scheme in GEOS-Chem is based on Fisher et al. (2016). The scheme includes two lumped monoterpenes (single- and double-bonded species) that are oxidized by OH,  $O_3$ , and  $NO_3$ , and the resulting peroxy radicals are oxidized to form second-generation products. The rates, products, and branching ratios for these reactions are all uncertain, and as such, the exact reason for the model glyoxal underestimation is not clear. The ultimate impact of this underestimation on the global glyoxal budget is small, due to the small contribution monoterpenes make to the total burden (Table 2); however, it is locally important in the boreal regions. Furthermore, a poor understanding of monoterpene oxidation (as indicated by glyoxal formation here) may also limit our ability to characterize ozone and secondary organic aerosol formation in these regions and reduce the quality of model air quality and climate predictions. This result underscores the need for an improved understanding of non-isoprene-dominated VOC chemistry, as recently suggested by Porter et al. (2017).

## 6. Conclusions

In this work, we use the GEOS-Chem model and satellite retrievals of glyoxal and formaldehyde to explore the global sources of glyoxal. To complete this work, we updated the GEOS-Chem glyoxal simulation, including additional chemical formation processes of glyoxal and its precursors, as well as updating direct emissions of glyoxal and its precursors. We use this model configuration to quantify the relative contribution of glyoxal production through five distinct chemical pathways and direct emissions. The simulated glyoxal production over biomass burning and isoprene-, aromatic-, and glycolaldehyde-dominated regions are qualitatively in

line with the OMI observations. However, low glyoxal production from aromatics may be responsible for the underestimation of glyoxal over Europe and China. Our analysis indicates that model glyoxal production from monoterpenes over boreal forests is biased substantially low (by a factor 3). This highlights the utility of the RGF as a constraint on VOC production and that uncertainties on simulated monoterpene chemistry are large, implying more work is needed to understand their oxidation mechanisms. Our analysis also suggests that the RGF from polar-orbiting satellite instruments may not be a strong proxy for glyoxal source types given the similarity of RGF values obtained over all source regions except those with significant glyoxal production from monoterpenes.

Ultimately, global data products, such as the OMI satellite retrievals used in this work, can provide valuable constraints on the global production of VOCs like glyoxal. They present an important opportunity for understanding the state of atmospheric VOCs and observing global change to the chemical sources of VOCs. As the bias and skew of these products are assessed, more rigorous constraints may be applied to the results found in this work. With the impending launch of the TEMPO satellite mission and other geostationary satellites, increased sampling will likely reduce the limiting uncertainties present here and allow for improved characterization of glyoxal sources and constraints on VOC precursors across the globe.

## Acknowledgments

This work was supported by NASA Headquarters under the NASA Earth and Space Science Fellowship Program Grant NNX16AN92H and by the National Science Foundation (ATM-1564495). The authors have no real or perceived financial conflicts of interests. OMI Formaldehyde data are available online at [https://disc.gsfc.nasa.gov/datasets/OMHCHO\\_V003/summary](https://disc.gsfc.nasa.gov/datasets/OMHCHO_V003/summary). The OMI Glyoxal data are available online at <https://avdc.gsfc.nasa.gov/pub/data/satellite/Aura/OMI/V03/L2/OMCHOCHO/>.

## References

- Atkinson, R., & Arey, J. (2003). Atmospheric degradation of volatile organic compounds. *Chemical Reviews*, 103(12), 4605–4638. <https://doi.org/10.1021/cr0206420>
- Bey, I., Jacob, D. J., Yantosca, R. M., Logan, J. A., Field, B. D., Fiore, A. M., et al. (2001). Global modeling of tropospheric chemistry with assimilated meteorology: Model description and evaluation. *Journal of Geophysical Research*, 106(D19), 23,073–23,095. <https://doi.org/10.1029/2001JD000807>
- Burkholder, J. B., Sander, S. P., Abbatt, J., Barker, J. R., Huie, R. E., Kolb, C. E., et al. (2015). Chemical kinetics and photochemical data for use in atmospheric studies, evaluation no. 18, JPL Publication 15–10, Jet Propulsion Laboratory, Pasadena. <http://jpldataeval.jpl.nasa.gov>
- Chan Miller, C., Gonzalez Abad, G., Wang, H., Liu, X., Kurosu, T., Jacob, D. J., & Chance, K. (2014). Glyoxal retrieval from the Ozone Monitoring Instrument. *Atmospheric Measurement Techniques*, 7(11), 3891–3907. <https://doi.org/10.5194/amt-7-3891-2014>
- Chan Miller, C., Jacob, D. J., González Abad, G., & Chance, K. (2016). Hotspot of glyoxal over the Pearl River Delta seen from the OMI satellite instrument: Implications for emissions of aromatic hydrocarbons. *Atmospheric Chemistry and Physics*, 16(7), 4631–4639. <https://doi.org/10.5194/acp-16-4631-2016>
- Chan Miller, C., Jacob, D. J., Marais, E. A., Yu, K., Travis, K. R., Kim, P. S., et al. (2017). Glyoxal yield from isoprene oxidation and relation to formaldehyde: Chemical mechanism, constraints from SENEX aircraft observations, and interpretation of OMI satellite data. *Atmospheric Chemistry and Physics*, 17(14), 8725–8738. <https://doi.org/10.5194/acp-17-8725-2017>
- Cohen, A. J., Brauer, M., Burnett, R., Anderson, H. R., Frostad, J., Estep, K., et al. (2017). Estimates and 25-year trends of the global burden of disease attributable to ambient air pollution: An analysis of data from the Global Burden of Diseases Study 2015. *The Lancet*, 389(10082), 1907–1918. [https://doi.org/10.1016/S0140-6736\(17\)30505-6](https://doi.org/10.1016/S0140-6736(17)30505-6)
- DiGangi, J. P., Henry, S. B., Kammrath, A., Boyle, E. S., Kaser, L., Schnitzhofer, R., et al. (2012). Observations of glyoxal and formaldehyde as metrics for the anthropogenic impact on rural photochemistry. *Atmospheric Chemistry and Physics*, 12(20), 9529–9543. <https://doi.org/10.5194/acp-12-9529-2012>
- Duncan, B. N., Prados, A. I., Lamsal, L. N., Yang, L., Streets, D. G., Gupta, P., et al. (2014). Satellite data of atmospheric pollution for U.S. air quality applications: Examples of applications, summary of data end-user resources, answers to FAQs, and common mistakes to avoid. *Atmospheric Environment*, 94, 647–662. <https://doi.org/10.1016/j.atmosenv.2014.05.061>
- Environmental Protection Agency National Emissions Inventory (2015). (National Emissions Inventory v1): Air Pollutant Emission Trends Data, Retrieved from <http://www.epa.gov/ttn/chieftrends/index.html> last access: 23 June 2015
- Fischer, E. V., Jacob, D. J., Yantosca, R. M., Sulprizio, M. P., Millet, D. B., Mao, J., et al. (2014). Atmospheric peroxyacetyl nitrate (PAN): A global budget and source attribution. *Atmospheric Chemistry and Physics*, 14(5), 2679–2698. <https://doi.org/10.5194/acp-14-2679-2014>
- Fisher, J. A., Jacob, D. J., Travis, K. R., Kim, P. S., Marais, E. A., Chan Miller, C., et al. (2016). Organic nitrate chemistry and its implications for nitrogen budgets in an isoprene- and monoterpene-rich atmosphere: Constraints from aircraft (SEAC4RS) and ground-based (SOAS) observations in the southeast US. *Atmospheric Chemistry and Physics*, 16(9), 5969–5991. <https://doi.org/10.5194/acp-16-5969-2016>
- Fortems-Cheiney, A., Chevallier, F., Pison, I., Bousquet, P., Saunio, M., Szopa, S., et al. (2012). The formaldehyde budget as seen by a global-scale multi-constraint and multi-species inversion system. *Atmospheric Chemistry and Physics*, 12(15), 6699–6721. <https://doi.org/10.5194/acp-12-6699-2012>
- Fu, T.-M., Jacob, D. J., Palmer, P. I., Chance, K., Wang, Y. X., Barletta, B., et al. (2007). Space-based formaldehyde measurements as constraints on volatile organic compound emissions in East and South Asia and implications for ozone. *Journal of Geophysical Research*, 112, D06312. <https://doi.org/10.1029/2006JD007853>
- Fu, T.-M., Jacob, D. J., Wittrock, F., Burrows, J. P., Vrekoussis, M., & Henze, D. K. (2008). Global budgets of atmospheric glyoxal and methylglyoxal, and implications for formation of secondary organic aerosols. *Journal of Geophysical Research*, 113, D15303. <https://doi.org/10.1029/2007JD009505>
- Gelaro, R., McCarty, W., Suárez, M. J., Todling, R., Molod, A., Takacs, L., et al. (2017). The Modern-Era Retrospective Analysis for Research and Applications, version 2 (MERRA-2). *Journal of Climate*, 30(14), 5419–5454. <https://doi.org/10.1175/JCLI-D-16-0758.1>
- Giglio, L., Randerson, J. T., & van der Werf, G. R. (2013). Analysis of daily, monthly, and annual burned area using the Fourth-Generation Global Fire Emissions Database (GFED4). *Journal of Geophysical Research: Biogeosciences*, 118, 317–328. <https://doi.org/10.1002/jgrg.20042>
- González Abad, G., Liu, X., Chance, K., Wang, H., Kurosu, T. P., & Suleiman, R. (2015). Updated Smithsonian Astrophysical Observatory Ozone Monitoring Instrument (SAO OMI) formaldehyde retrieval. *Atmospheric Measurement Techniques*, 8(1), 19–32. <https://doi.org/10.5194/amt-8-19-2015>

- Guenther, A. B., Jiang, X., Heald, C. L., Sakulyanontvittaya, T., Duhl, T., Emmons, L. K., & Wang, X. (2012). The Model of Emissions of Gases and Aerosols from Nature version 2.1 (MEGAN2.1): an extended and updated framework for modeling biogenic emissions. *Geoscientific Model Development*, 5, 1471–1492. <https://doi.org/10.5194/gmd-5-1471-2012>
- Hirsch, R. M., & Gilroy, E. J. (1984). Methods of fitting a straight line to data: Examples in water Resources. *JAWRA Journal of the American Water Resources Association*, 20(5), 705–711. <https://doi.org/10.1111/j.1752-1688.1984.tb04753.x>
- Intergovernmental Panel on Climate Change (2013). In T. F. Stocker, D. Qin, G.-K. Plattner, M. Tignor, S. K. Allen, J. Boschung, et al. (Eds.), *Climate change 2013: The physical science basis. Contribution of Working Group I to the Fifth Assessment Report of the Intergovernmental Panel on Climate Change*. Cambridge, United Kingdom and New York, NY: Cambridge University Press.
- Kaiser, J., Jacob, D. J., Zhu, L., Travis, K. R., Fisher, J. A., González Abad, G., et al. (2018). High-resolution inversion of OMI formaldehyde columns to quantify isoprene emission on ecosystem-relevant scales: Application to the southeast US. *Atmospheric Chemistry and Physics*, 18(8), 5483–5497. <https://doi.org/10.5194/acp-18-5483-2018>
- Kaiser, J., Kaiser, J., Wolfe, G. M., Min, K. E., Brown, S. S., Miller, C. C., et al. (2015). Reassessing the ratio of glyoxal to formaldehyde as an indicator of hydrocarbon precursor speciation. *Atmospheric Chemistry and Physics*, 15(13), 7571–7583. <https://doi.org/10.5194/acp-15-7571-2015>
- Knote, C., Hodzic, A., Jimenez, J. L., Volkamer, R., Orlando, J. J., Baidar, S., et al. (2014). Simulation of semi-explicit mechanisms of SOA formation from glyoxal in aerosol in a 3-D model. *Atmospheric Chemistry and Physics*, 14(12), 6213–6239. <https://doi.org/10.5194/acp-14-6213-2014>
- Li, M., Zhang, Q., Kurokawa, J. I., Woo, J. H., He, K., Lu, Z., et al. (2017). MIX: A mosaic Asian anthropogenic emission inventory under the international collaboration framework of the MICS-Asia and HTAP. *Atmospheric Chemistry and Physics*, 17(2), 935–963. <https://doi.org/10.5194/acp-17-935-2017>
- Li, M., Zhang, Q., Streets, D. G., He, K. B., Cheng, Y. F., Emmons, L. K., et al. (2014). Mapping Asian anthropogenic emissions of non-methane volatile organic compounds to multiple chemical mechanisms. *Atmospheric Chemistry and Physics*, 14(11), 5617–5638. <https://doi.org/10.5194/acp-14-5617-2014>
- Mao, J., Paulot, F., Jacob, D. J., Cohen, R. C., Crounse, J. D., Wennberg, P. O., et al. (2013). Ozone and organic nitrates over the eastern United States: Sensitivity to isoprene chemistry. *Journal of Geophysical Research: Atmospheres*, 118, 11,256–11,268. <https://doi.org/10.1002/jgrd.50817>
- Marais, E. A., Jacob, D. J., Guenther, A., Chance, K., Kurosu, T. P., Murphy, J. G., et al. (2014). Improved model of isoprene emissions in Africa using Ozone Monitoring Instrument (OMI) satellite observations of formaldehyde: Implications for oxidants and particulate matter. *Atmospheric Chemistry and Physics*, 14(15), 7693–7703. <https://doi.org/10.5194/acp-14-7693-2014>
- Marais, E. A., Jacob, D. J., Jimenez, J. L., Campuzano-Jost, P., Day, D. A., Hu, W., et al. (2016). Aqueous-phase mechanism for secondary organic aerosol formation from isoprene: Application to the southeast United States and co-benefit of SO<sub>2</sub> emission controls. *Atmospheric Chemistry and Physics*, 16(3), 1603–1618. <https://doi.org/10.5194/acp-16-1603-2016>
- Marvin, M. R., Wolfe, G. M., Salawitch, R. J., Canty, T. P., Roberts, S. J., Travis, K. R., Aikin, Kenneth C., et al. (2017). Impact of evolving isoprene mechanisms on simulated formaldehyde: An inter-comparison supported by in situ observations from SENEX. *Atmospheric Environment*, 164, 325–336. <https://doi.org/10.1016/j.atmosenv.2017.05.049>
- Mu, M., Randerson, J. T., van der Werf, G. R., Giglio, L., Kasibhatla, P., Morton, D., et al. (2011). Daily and 3-hourly variability in global fire emissions and consequences for atmospheric model predictions of carbon monoxide. *Journal of Geophysical Research*, 116, D24303. <https://doi.org/10.1029/2011JD016245>
- Myriokefalitakis, S., Vrekoussis, M., Tsigaridis, K., Wittrock, F., Richter, A., Brühl, C., et al. (2008). The influence of natural and anthropogenic secondary sources on the glyoxal global distribution. *Atmospheric Chemistry and Physics*, 8(16), 4965–4981. <https://doi.org/10.5194/acp-8-4965-2008>
- Palmer, P. I., Jacob, D. J., Chance, K., Martin, R. V., Spurr, R. J. D., Kurosu, T. P., et al. (2001). Air mass factor formulation for spectroscopic measurements from satellites: Application to formaldehyde retrievals from the Global Ozone Monitoring Experiment. *Journal of Geophysical Research*, 106(D13), 14,539–14,550. <https://doi.org/10.1029/2000JD900772>
- Porter, W. C., Safieddine, S. A., & Heald, C. L. (2017). Impact of aromatics and monoterpenes on simulated tropospheric ozone and total OH reactivity. *Atmospheric Environment*, 169, 250–257. <https://doi.org/10.1016/j.atmosenv.2017.08.048>
- Safieddine, S. A., Heald, C. L., & Henderson, B. H. (2017). The Global non-methane reactive organic carbon budget: A modeling perspective. *Geophysical Research Letters*, 44, 3897–3906. <https://doi.org/10.1002/2017GL072602>
- Schultz, M., Backman, L., Balkanski, Y., Bjoerndalsaeter, S., Brand, R., Burrows, J., et al. (2007). REanalysis of the TROpospheric chemical composition over the past 40 years (RETRO)—A long-term global modeling study of tropospheric chemistry: Final report, Jülich/Hamburg, Germany.
- Simone, N. W., Stettler, M. E. J., & Barrett, S. R. H. (2012). Rapid estimation of global civil aviation emissions with uncertainty quantification. *Transportation Research Part D: Transport and Environment*, 25, 33–41.
- Stettler, M. E. J., Eastham, S., & Barrett, S. R. H. (2011). Air quality and public health impacts of UK airports. Part I: Emissions. *Atmospheric Environment*, 45, 5415–5424.
- Surl, L., Palmer, P. I., & González Abad, G. (2018). Which processes drive observed variations of HCHO columns over India? *Atmospheric Chemistry and Physics*, 18(7), 4549–4566. <https://doi.org/10.5194/acp-18-4549-2018>
- Travis, K. R., Jacob, D. J., Fisher, J. A., Kim, P. S., Marais, E. A., Zhu, L., et al. (2016). Why do models overestimate surface ozone in the Southeast United States? *Atmospheric Chemistry and Physics*, 16(21), 13,561–13,577. <https://doi.org/10.5194/acp-16-13561-2016>
- Volkamer, R., Molina, L. T., Molina, M. J., Shirley, T., & Brune, W. H. (2005). DOAS measurement of glyoxal as an indicator for fast VOC chemistry in urban air. *Geophysical Research Letters*, 32, L08806. <https://doi.org/10.1029/2005GL022616>
- Volkamer, R., San Martini, F., Molina, L. T., Salcedo, D., Jimenez, J. L., & Molina, M. J. (2007). A missing sink for gas-phase glyoxal in Mexico City: Formation of secondary organic aerosol. *Geophysical Research Letters*, 34, L19807. <https://doi.org/10.1029/2007GL030752>
- Vrekoussis, M., Wittrock, F., Richter, A., & Burrows, J. P. (2009). Temporal and spatial variability of Glyoxal as observed from space. *Atmospheric Chemistry and Physics*, 9(13), 4485–4504. <https://doi.org/10.5194/acp-9-4485-2009>
- Vrekoussis, M., Wittrock, F., Richter, A., & Burrows, J. P. (2010). GOME-2 observations of oxygenated VOCs: What can we learn from the ratio glyoxal to formaldehyde on a global scale? *Atmospheric Chemistry and Physics*, 10(21), 10,145–10,160. <https://doi.org/10.5194/acp-10-10145-2010>
- Wittrock, F., Richter, A., Oetjen, H., Burrows, J. P., Kanakidou, M., Myriokefalitakis, S., et al. (2006). Simultaneous global observations of glyoxal and formaldehyde from space. *Geophysical Research Letters*, 33, L16804. <https://doi.org/10.1029/2006GL026310>
- Yang, X., Xue, L., Wang, T., Wang, X., Gao, J., Lee, S., et al. (2018). Observations and explicit modeling of summertime carbonyl formation in Beijing: Identification of key precursor species and their impact on atmospheric oxidation chemistry. *Journal of Geophysical Research: Atmospheres*, 123, 1426–1440. <https://doi.org/10.1002/2017JD027403>



- Yevich, R., & Logan, J. A. (2003). An assessment of biofuel use and burning of agricultural waste in the developing world. *Global Biogeochemical Cycles*, 17(4), 1095. <https://doi.org/10.1029/2002GB001952>
- Zarzana, K. J., Min, K.-E., Washenfelder, R. A., Kaiser, J., Krawiec-Thayer, M., Peischl, J., et al. (2017). Emissions of glyoxal and other carbonyl compounds from agricultural biomass burning plumes sampled by aircraft. *Environmental Science & Technology*, 51(20), 11,761–11,770. <https://doi.org/10.1021/acs.est.7b03517>
- Zhu, L., Jacob, D. J., Kim, P. S., Fisher, J. A., Yu, K., Travis, K. R., et al. (2016). Observing atmospheric formaldehyde (HCHO) from space: Validation and intercomparison of six retrievals from four satellites (OMI, GOME2A, GOME2B, OMPS) with SEAC4RS aircraft observations over the southeast US. *Atmospheric Chemistry and Physics Discussions*, 14, 1–24. <https://doi.org/10.5194/acp-2016-162>